Heat and Mass Transfer 34 (1998) 337–347 © Springer-Verlag 1998

Solidification of hypereutectic and hypoeutectic binary alloys with buoyancy and surface tension driven natural convection

M. A. Rady, S. A. Nada

Abstract Convection patterns and evolution of macrosegregation during solidification of hypereutectic and hypoeutectic NH_4CL-H_2O binary systems in rectangular side chilled ingots have been numerically investigated. Under the conditions of pure thermal/solutal convection, without a free surface, solidification of NH_4CL 70%-H_2O hypereutectic alloy is characterized by the formation of channels and A-segregates, while solidification of NH_4CL 10%-H_2O hypoeutectic alloy is characterized by the formation of circulation cells in the narrow melt and V-segregates. Surface tension effects during solidification of NH_4CL 70%-H_2O results in establishing a counterclockwise rotating cell at the cavity top, changing the number and orientation of developed channels, and creating an area of negative segregation at the cavity top. During solidification of NH_4CL 10%-H_2O, surface tension effects increase the intensity of flow and results in a higher degree of macrosegregation.

List of symbols

C	specific heat (J/kg. K)
D	continuum mass diffusion coefficient (m^2/s)
f	mass fraction of solid or liquid phase
f_k^α	mass fraction of constituent α in phase k
f_m^α	mass fraction of constituent α in the mixture
g	volume fraction or gravitational acceleration (m/s^2)
h	enthalpy (J/kg)
k	continuum thermal conductivity (W/m. K)
K	permeability (m^2)
K_o	permeability coefficient (m^2)
Le	Lewis number (α/D)
P	pressure (N/m^2)
Ma_s	solutal Marangoni number, $(-\sigma_s(f_l^\alpha - f_{l,o}^\alpha)L/\mu_l\alpha_l)$
Ma_T	thermal Marangoni number $(-\sigma_T(T - T_o)L/\mu_l\alpha_l)$
S	source term
t	time (s)
T	temperature (K)
u, v	velocity components in x and y directions (m/s)
u_m, v_m	mixture mass averaged velocities in x and y directions
V	velocity vector
V_k	mass averaged velocity of phase k
V_m	mixture mass averaged velocity
x, y	Cartesian coordinates

Greek symbols

α	thermal diffusivity (m^2/s)
β_T	thermal expansion coefficient (l/K)
β_C	solutal expansion coefficient
ϕ	general dependent scalar variable
Γ	general diffusion coefficient (m^2/s)
μ	dynamic viscosity (Pa.s)
ρ	density (kg/m^3)
σ_s	solutal surface tension gradient (N/m)
σ_T	thermal surface tension gradient (N/m K)

Subscripts

C	cold boundary
i	initial
k	phase k
l	liquid
m	mixture
o	reference conditions
s	solid

Superscripts

α	constituent α

Received on 9 June 1998

M. A. Rady, S. A. Nada
Department of Mechanical Engineering Technology
Benha High Institute of Technology, Benha 13512-Egypt

Correspondence to: M. A. Rady

1 Introduction

Heat transfer during melting and solidification is of particular interest in materials processing, solidification of castings and ingots, welding, and many other applications. During solidification of a binary alloy, the solute is rejected from the solidifying dendrites and accumulates in the adjoining liquid, establishing local concentration gradients. Thermosolutal convection is induced due to buoyancy forces resulting from temperature and concentration gradients. Convection may be also driven by surface tension gradients resulting from temperature and/or concentration gradients along a free surface. The resulting surface motion is termed thermo/diffusocapillary convection.

Studies on thermosolutal convection during solidification of binary alloys [1–4] have revealed different physical features of the process. These physical features include development of an irregular liquidus front, remelting of solid, development of flow channels in the mushy region, and establishment of characteristic macrosegregation

patterns in the final solid. Detailed discussion of the transport mechanisms and a comprehensive review can be found in the recent publications [5–8].

Studies on surface tension effects have concentrated largely on flows without phase change. Numerical simulations of thermocapillary convection in a differentially heated rectangular cavity without natural convection [9–11] show that the maximum velocity occurs near the intersection of the free surface with the cold side wall, where the thermocapillary driven flow is turned by the wall. A zero gravity simulation of thermo/diffusocapillary convection performed by T. L. Bergman [12] show the formation of counterrotating solutally and thermally driven cells for equal but opposite values of the thermal and Marangoni numbers. Calculations performed for combined thermocapillary convection and thermal natural convection in a rectangular cavity [13, 14] show that augmenting surface tension and buoyancy forces enhance fluid velocities, while opposing forces result in multicellular flows.

The effects of augmenting buoyancy and surface tension forces on solidification of a pure substance have been studied by Keller and Bergman [15]. Thermocapillary flows were predicted to reduce solidification at the free surface. Numerical analysis of the effects of thermo/diffusocapillary convection on the solidification of NH_4CL-H_2O hypereutectic binary system in a differentially heated square cavity has been performed by Incropera et al. [16]. Surface tension effects have been found to influence the fluid flow and interface morphology primarily during early and intermediate stages of solidification.

Solidification of hypereutectic and hypoeutectic alloys differs in many ways. During solidification of hypereutectic alloys, the rejection of solute-rich interdendritic fluid results in solutally and thermally driven flows opposing each other. For hypoeutectic alloys, the solutal and thermal buoyancy forces are augmenting each other. Also, the surface tension forces along the free surface may augment or oppose the buoyancy forces. Hence, different flow patterns are induced depending on the initial concentration of the alloy. Solidification of hypereutectic and hypoeutectic NH_4CL-H_2O binary systems in rectangular side chilled ingots, without a free surface, have been numerically investigated by Rady et al. [17]. Solidification of NH_4CL 70%-H_2O hypereutectic alloys is characterized by the formation of channels and A-segregates. During solidification of NH_4CL 10%-H_2O hypoeutectic alloy, the formation of circulation cells at the liquidus interface at later stages of the process were shown to be responsible for the development of V shaped segregates in the final casting.

The objective of the studies reported in the present paper is to examine convection patterns and macrosegregation during solidification of hypereutectic and hypoeutectic NH_4CL-H_2O binary system in a rectangular side chilled ingot with both buoyancy and surface tension forces. The results for both the binary systems are compared with the base case of solidification in the absence of a free surface, without surface tension driven convection.

2
Physical model

Solidification of aqueous ammonium chloride (NH_4CL-H_2O) system, which exhibits a dendritic growth behavior and is analogous to a large class of metal alloys, is considered in the present study. A mixture of uniform initial composition f_i^{α} and temperature T_i is contained in the cavity, see Fig. 1. Solidification starts by chilling the left wall to a temperature T_C, lower than the eutectic temperature T_e. The right wall is considered to be insulated because it is either the uncooled surface of an ingot cooled from the side (unidirectional solidification) or the central plane of symmetry in an ingot cooled from both sides. Top and bottom walls are considered to be insulated. Two initial concentrations 30% and 10% of NH_4CL have been considered. By referring to the phase diagram, Fig. 2, these concentrations correspond to solutions located to the right (hypereutectic) and to the left (hypoeutectic) of the eutectic point (19.7% NH_4CL). Thermophysical properties of NH_4CL-H_2O and operating conditions are shown in Table 1.

3
Governing equations and solution procedure

Simulations of the present study are based on the continuum model for transport phenomena in dendritic solidification systems [18, 19]. The continuum conservation equations are written in general form as follows.

$$\frac{\partial}{\partial t}(\rho\phi_m) + \nabla\cdot(\rho V_m\phi_m) = \nabla\cdot(\Gamma_\phi\nabla\phi_m) + S_\phi \qquad (1)$$

Where ϕ_m, Γ_ϕ and S_ϕ represent different terms in the equations as stated below

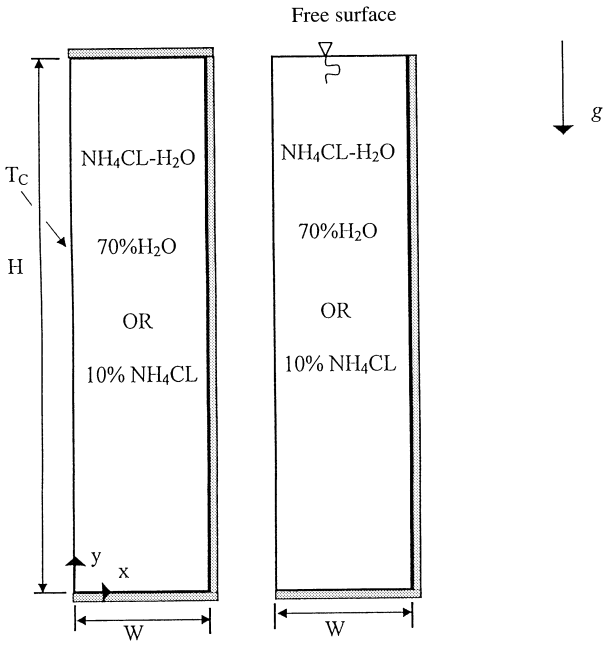

a Without a free surface **b** With a free surface

Fig. 1. Solidification of NH_4CL-H_2O in a statically cast ingot, physical models

Equation	ϕ_m	Γ_ϕ	S_ϕ
Continuity	1	0	0
x-Momentum	u_m	μ	$-\frac{\mu}{K}(u_m - u_s) - \frac{\partial P}{\partial x}$
y-Momentum	v_m	μ	$-\frac{\mu}{K}(v_m - v_s) + \rho_l g(\beta_T(T - T_o) + \beta_C(f_l^\alpha - f_l^\alpha)) - \frac{\partial P}{\partial y}$
Energy	h_m	k/c	$\nabla \cdot (\frac{k}{c_s}\nabla(h_s - h_m)) - \nabla \cdot (\rho(h_l - h_m)(V_m - V_s))$
Species	f_m^α	ρD	$\nabla \cdot \left(\rho D \nabla(f_l^\alpha - f_m^\alpha)\right) - \nabla \cdot \left(\rho(f_l^\alpha - f_m^\alpha)(V_m - V_s)\right)$

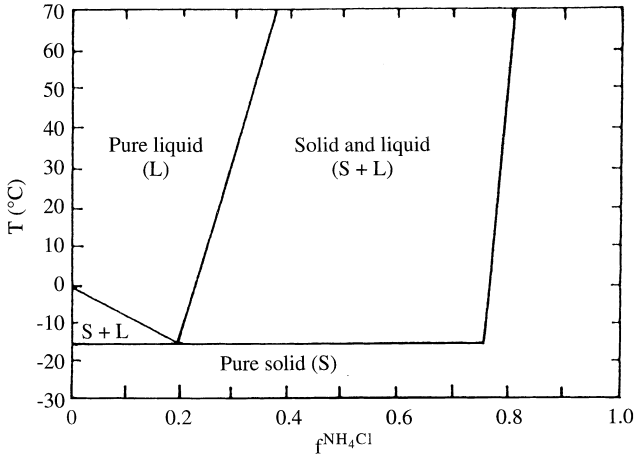

Fig. 2. Equilibrium phase diagram for NH_4CL-H_2O system

Mean mixture theory is used to define the continuum density, velocity, enthalpy and species mass fraction. These definitions and the simplifying assumptions invoked may be found in [18, 19]. The isotropic permeability from the Blake-Kozeny equation [18, 20] is given by

$$K = \frac{K_o g_l^3}{(1 - g_l)^2} \tag{2}$$

where K_o is a constant, which depends on the specific multiphase region morphology.

Since the energy and species conservation equations are written in terms of mixture enthalpy and mixture concentration, supplemental relations are needed to obtain the local temperature, phase fractions, and phase compositions from the knowledge of the mixture enthalpy and mixture composition. These relations are obtained from the equilibrium phase diagram under the assumptions of thermal and chemical equilibrium [18, 20]. Details of the solution procedure have been reported by Rady [21].

Hydrodynamic boundary conditions include the zero-slip requirement for the side walls and cavity bottom and a balance between shear and surface tension forces at the free surface.

$$\mu \left.\frac{\partial u}{\partial y}\right|_{y=H} = \sigma_T \left.\frac{\partial T}{\partial x}\right|_{y=H} + \sigma_s \left.\frac{\partial f_l^\alpha}{\partial x}\right|_{y=H} \tag{3}$$

All surfaces are impermeable with respect to momentum and species transfer. Thermal boundary conditions correspond to isothermal side-left wall and adiabatic right, top and bottom walls. The shear stress on the left-hand side of Eq. (3) is responsible for the surface tension convection and occurs whenever the surface tension of the liquid phase varies with temperature and concentration. The surface tension for an aqueous NH_4CL solution increases with decreasing temperature and water composition. Appropriate values for the thermal and solutal surface tension gradients are $\sigma_T = -0.15 \times 10^{-3}$ N/m K and $\sigma_s = -0.283 \times 10^{-1}$ N/m.

Table 1. Thermophysical properties of NH_4CL-H_2O and operating conditions

	NH_4CL-70% H_2O		NH_4CL-10% H_2O	
	Solid	Liquid	Solid	Liquid
Specific heat (J/kg K)	1870	3249	2184	3795
Thermal conductivity (W/m K)	0.393	0.468	0.393	0.468
Density (kg/m^3)	1078	1078	1033	1033
Diffusion coefficient (m^2/s)	–	4.8×10^{-9}	–	0.9×10^{-9}
Viscosity (kg/m s)	–	1.3×10^{-3}	–	0.82×10^{-3}
Latent heat of fusion (J/kg)	3.138×10^5		3.33×10^5	
Permeability coefficient, K_o (m^2)	5.56×10^{-11}		5.56×10^{-11}	
Thermal expansion coefficient, β_T (1/K)	3.832×10^{-4}		1.74×10^{-4}	
Solutal expansion coefficient, β_C	0.257		−0.3	
Eutectic compositions, f_e^α	0.803		0.197	
Eutectic Temperature, T_e (k)	257.75		257.75	
Zero composition melting point, T_m (K)	633.59		273.15	
Equilibrium partition ratio, k_p	0.3		0.0001	
Mold height/width, H/W (m/m)	0.1/0.025		0.1/0.025	
Initial temperature, T_i (K)	310.96		313.0	
Chill wall temperature, T_C (K)	223.0		223.0	
Initial composition, $f_{t,l}^\alpha$	0.7 H_2O		0.1 NH_4CL	

The governing equations have been discretized using the control volume finite difference method and power law convection-diffusion scheme has been employed. SIMPLER algorithm has been adopted for solution of the flow field [22]. The energy and species conservation equations are iterated during an overall iteration loop to first obtain a convergence in the local liquid fraction values. It is considered that the solution has converged when the local mass imbalance is less than 5×10^{-5} and the relative changes in the values of local enthalpy, concentration, and liquid fraction are less than 10^{-4}, 10^{-4}, and 10^{-5}, respectively. Details of the numerical scheme have been reported by Rady [21].

The code employing the present numerical scheme has been validated by comparison with the experimental and numerical results available in the literature for melting and solidification of pure metals in a cavity [23] and for solidification of NH_4CL-H_2O binary system [17].

4
Results and discussion

Numerical solutions obtained for solidification of NH_4CL-70% H_2O using 42×42, 52×52, and 62×62 uniform grids show a small difference in the convection and macrosegregation patterns predicted by the 52×52 and 62×62 grids. The 62×62 grid has been employed in the present study. Results of the numerical calculations for solidification of NH_4CL 70%-H_2O and NH_4CL 10%-H_2O are presented in the following sections. For each case, solidification in the rectangular ingot without a free surface is presented first and considered as the base case for comparison with the results obtained when a free surface is introduced. Flow patterns, represented by streamline plots, and the resultant macrosegregation at different times during solidification are discussed.

4.1
Solidification of NH_4CL 70%-H_2O, hypereutectic system

Rectangular ingot without a free surface

Plots of isotherms and liquid isocomposition lines at different times show that, in general, the minimum temperature and maximum liquid concentration are found near the cold wall and high concentration and temperature gradients are located within the mushy zone. Isotherms and isocomposition lines are not presented here for brevity. Streamlines plots after 240, 390, and 870 s of cooling are shown in Fig. 3. Streamlines are plotted using 20 equal intervals between the minimum and maximum values. The numbers between the brackets at the top of each plot are the minimum and maximum contour values, respectively. The dotted lines superimposed on streamlines plot represent the solidus and liquidus fronts.

High temperature gradients at the chilled wall result in initially strong counterclockwise circulation. The intensity of this thermally induced flow decreases as the melt near the insulated wall cools. As the solid forms, colder water enriched fluid is rejected from the mushy region. For $f_1^{\alpha} = 30\%$ NH_4CL (70% H_2O) hypereutectic alloy, the sol-

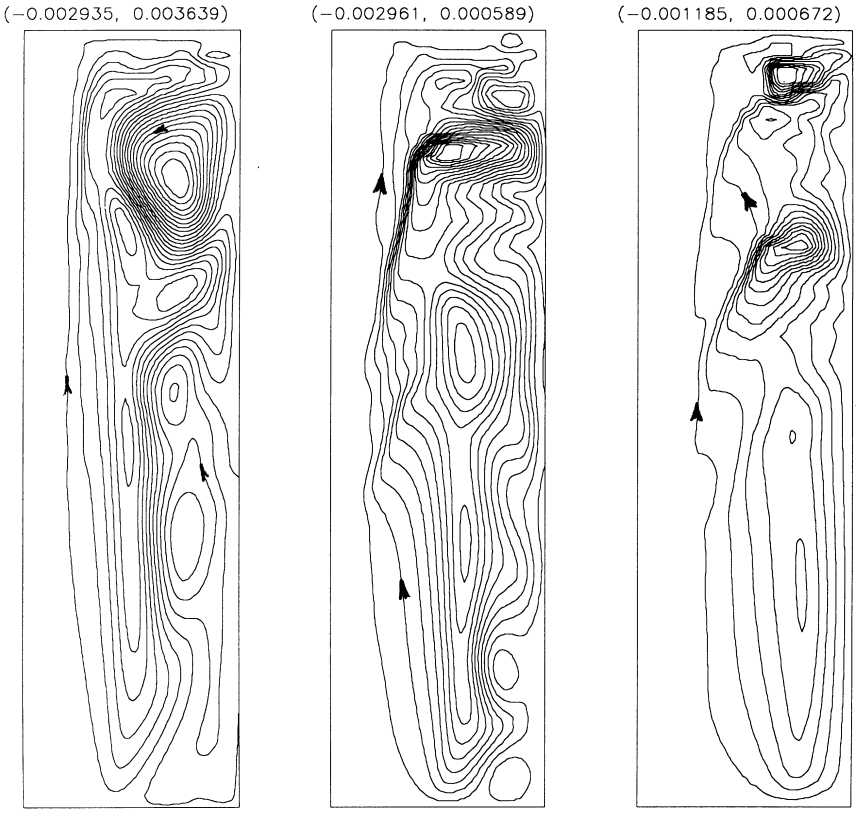

a 240 s **b** 390 s **c** 870 s

Fig. 3a–c. Convection conditions during solidification of NH_4CL 70%-H_2O without a free surface

ute H_2O is lighter than the solvent, both β_r and β_C are positive. The rejection of less dense water-rich interdendritic fluid results in solutally and thermally driven flows opposing each other. As can be seen in Fig. 3(a), the water rich fluid rises to the cavity top and moves horizontally across the top surface and is driven back to the liquidus by the stronger thermally driven flow. The conditions at the cavity top are double diffusive. Colder water-rich fluid is overlying warmer water-deficient fluid. And temperature and composition gradients are making opposing contributions to the vertical density distribution.

After 390 s, the solutally driven circulation is dominant. Water rich interdendritic fluid penetrates the liquidus interface towards the center of the casting at many locations. As it moves to the center it gets hotter. Since the liquid was in equilibrium with solid at a lower temperature, it can induce remelting. Local water enrichment by the penetrating interdendritic fluid results in local depression of the liquidus temperature. Localized melting of solid dendrites occurs, the permeability increases with increasing liquid fraction, and hence the flow resistance decreases. The flow follows preferred channels which are indicated by the closely spaced streamlines shown in Fig. 3(b, c). These channels manifest themselves in the final casting in the form of A-segregates.

The macrosegregation patterns at 390, 870, and 9200 s (complete solidification) are shown in Fig. 4. Regions of different H_2O concentration have been distinctly shown. In addition to the solute rich channels of positive segregation, the continued discharge of interdendritic fluid into the bulk fluid leads to the formation of a water rich region in the right top corner of the ingot forming cone segregate. The solute enrichment in these regions occurs at the expense of solute depleted regions in the bottom and at several locations in the middle of the cavity. With the passage of time, the cone segregate deepens, solute depleted bands in the middle enlarge and elongate adjacent to the solute rich A segregates, and the small solute depleted region at the bottom grows.

Rectangular ingot with a free surface

In addition to the existence of solutally and thermally driven flows opposing each other in the mushy zone, temperature and concentration gradients on the free surface create opposing thermocapillary and diffusocapillary effects. However, NH_4CL-H_2O is characterized by a large Lewis number (Le = 28). Hence, diffusocapillary effects are limited to the inner part of the mushy region, where the permeability is small and convection is suppressed. Also, $Ma_T/Ma_s \sim 2.5$, therefore thermally induced surface tension differences exceed solutally induced differences. These conditions are favoring thermocapillary effects.

Contrasting Figs. 3 and 5, it is shown that surface tension effects during solidification of NH_4CL 70%-H_2O results in establishing a counterclockwise rotating cell at the cavity top. This counterclockwise rotating cell is sustained by the large temperature gradients in this region. The capillary flow of warmer bulk fluid penetrates the permeable liquidus interface, causing a reduction in the local solidification rate and thinning of the liquidus front at the cavity top as compared to the base case. The momentum of the upward solutally driven flow along the solidus is not

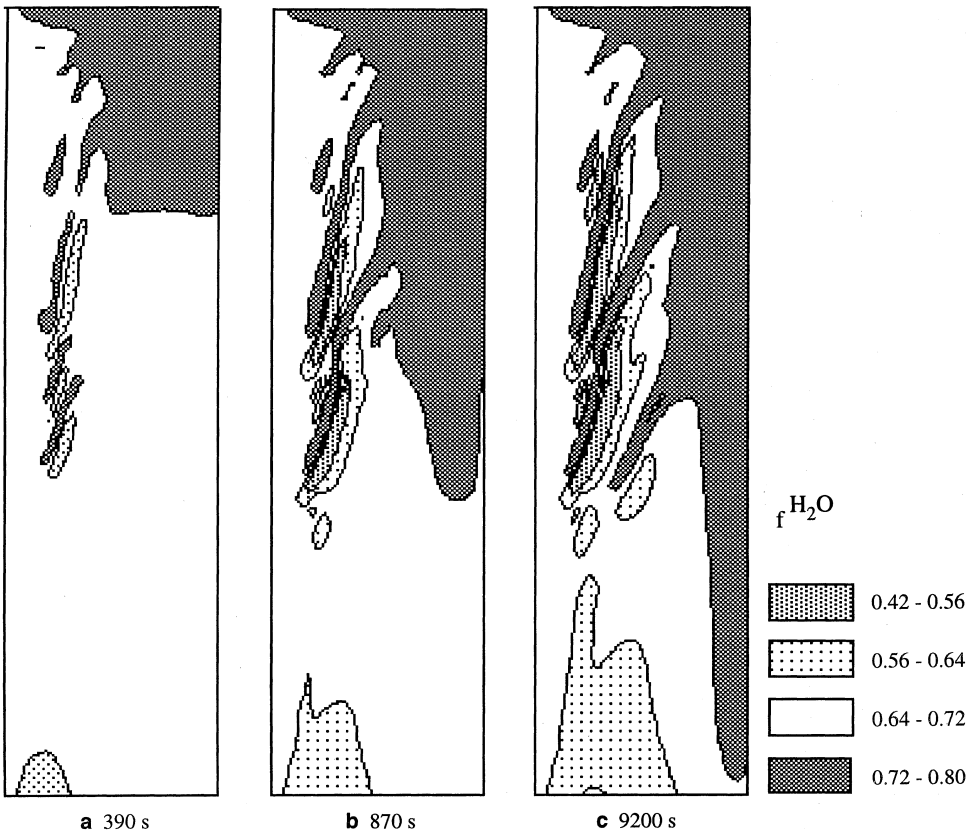

Fig. 4a–c. Development of macrosegregation with time during solidification of NH_4CL 70%-H_2O without a free surface

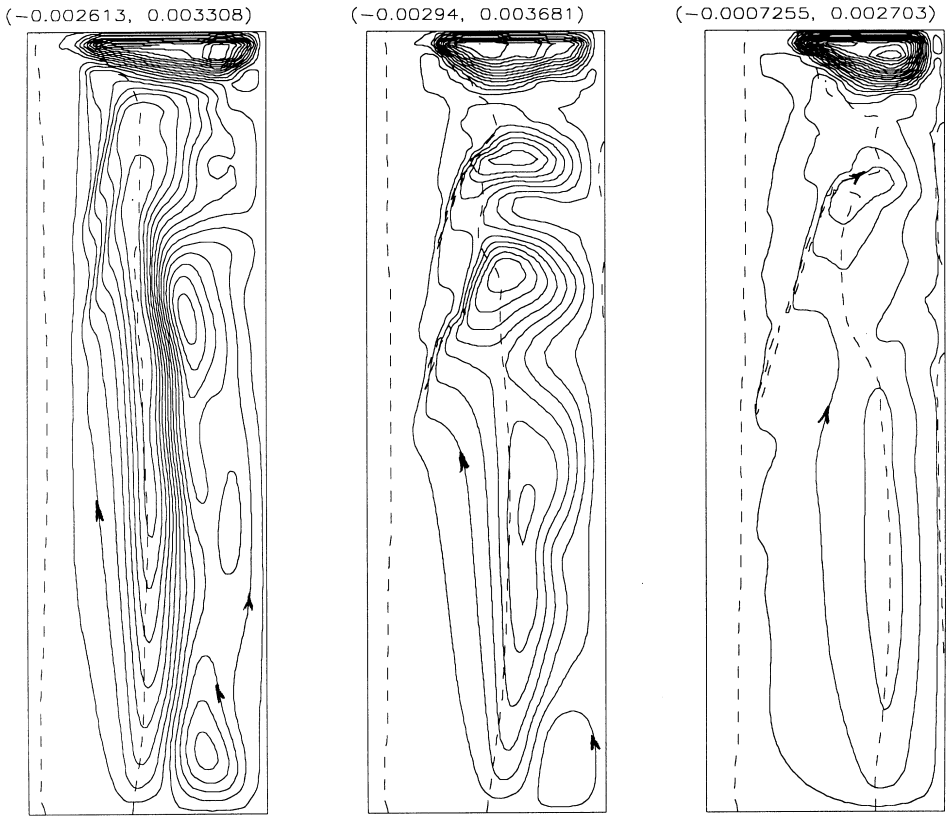

a 240 s **b** 390 s **c** 870 s

Fig. 5a–c. Convection conditions during solidification of NH_4CL 70%-H_2O with a free surface

sufficient to overcome the effects of capillary convection. Hence, the uprising water-rich fluid does not penetrate into the bulk fluid at the top of the cavity but at locations below the counterclockwise rotating cell. The thermally driven counterclockwise rotating cell near the cavity top, shown in Fig. 3a, is not present when a free surface is introduced. After 390 s of cooling, the solutally driven flow becomes dominant, within the mushy zone, and penetrates the liquidus front at many locations creating preferred flow channels, represented by the closely spaced streamlines in Fig. 5b, c. However, the number and orientation of these developed channels differs from the base case, shown in Fig. 3b, c.

The macrosegregation patterns at 390, 870, and 9200 s (complete solidification) are shown in Fig. 6. Comparison with the macrosegregation patterns predicted with pure natural convection, shown in Fig. 5, shows that an area of negative segregation is established at the cavity top in the presence of a free surface. This may be attributed to the presence of capillary flow at the cavity top, which carries the expelled water rich fluid from the mush to the bulk liquid. Areas of positive segregation in form of cone segregate and solute depleted regions at the cavity bottom are similar for the two cases. The difference in the number and orientation of solute rich bands adjacent to solute depleted bands, A-segregates, arising due to the formation of flow preferred channels during solidification, may be also noted.

The variation of maximum and minimum H_2O concentration with time during solidification with and without a free surface is shown in Table 2. It may be noted that, H_2O concentration attains its minimum value at earlier stages during solidification in the presence of a free surface, which is attributed to capillary flow at the cavity top. Values of maximum H_2O concentration are comparable for the two cases. At complete solidification, the minimum H_2O concentration in the presence of a free surface is slightly smaller than the value obtained without a free surface.

Table 2. Variation of minimum and maximum values of H_2O concentration with time during solidification of $NH_4CL70\%$-H_2O

Time (s)	240	390	870	9200
(a) Without a free surface				
$f_{\min}^{H_2O}$	0.614	0.534	0.433	0.4148
$f_{\max}^{H_2O}$	0.793	0.797	0.800	0.803
(b) With a free surface				
$f_{\min}^{H_2O}$	0.400	0.400	0.400	0.400
$f_{\max}^{H_2O}$	0.7872	0.7975	0.8005	0.803

4.2 Solidification of NH_4CL 10%-H_2O, hypoeutectic system

Rectangular ingot without a free surface

Convection conditions after 870 s, 1200 s, 2000 s of cooling are shown in Fig. 7. Streamlines are plotted using 10 equal intervals between the minimum and maximum

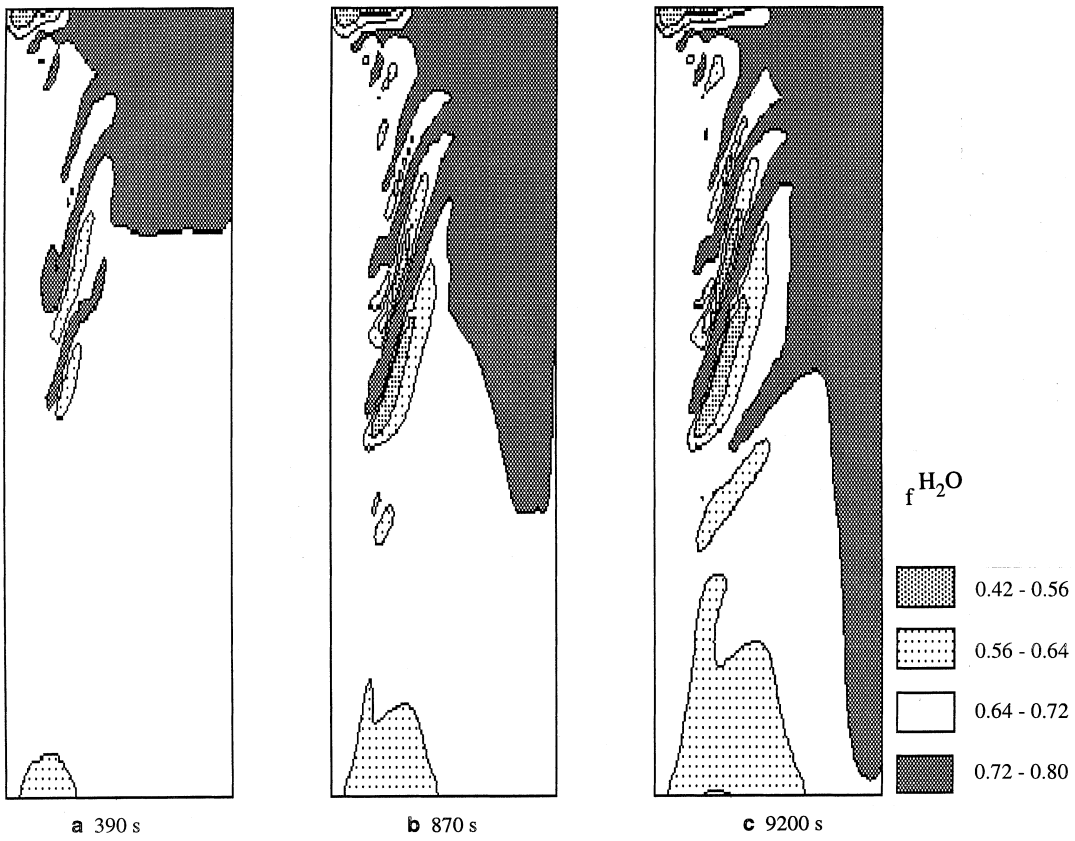

Fig. 6a–c. Development of macrosegregation with time during solidification of NH_4CL 70%-H_2O with a free surface

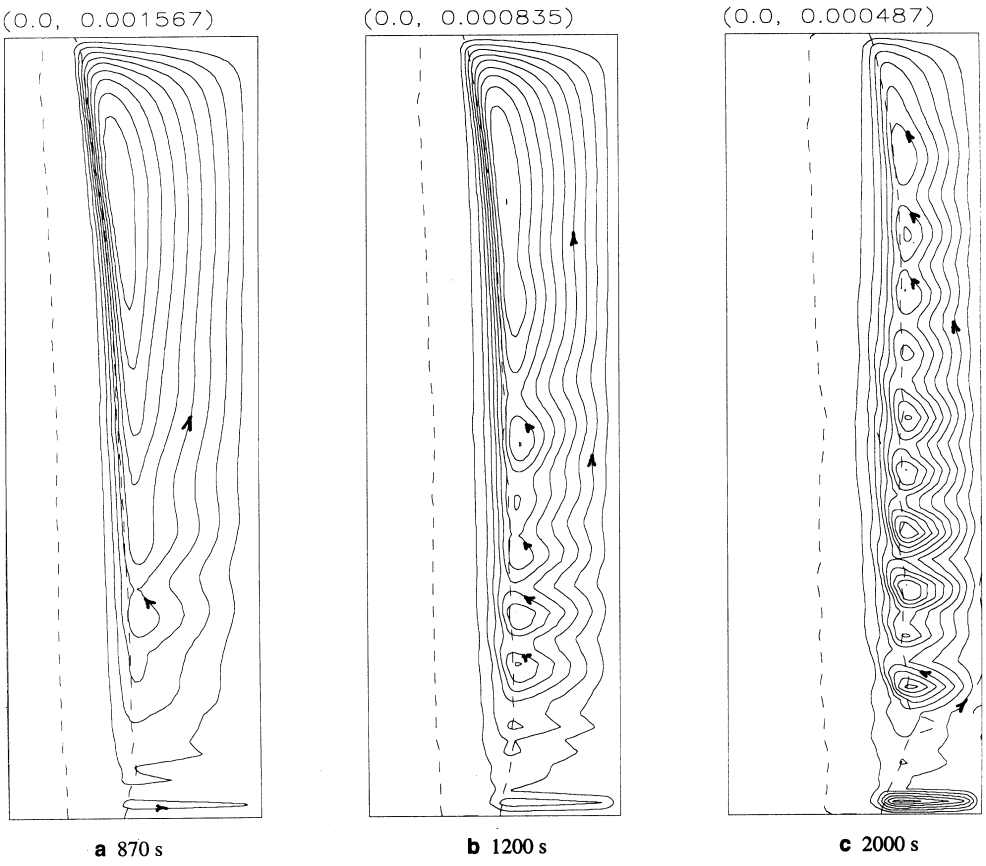

Fig. 7a–c. Convection conditions during solidification of NH_4CL 10%-H_2O without a free surface

contour values. At the beginning of the process, conditions are similar to those of thermally induced natural convection in a cavity. As solidification starts, NH_4CL enriched fluid is rejected from the mushy zone. For $f_l^{\alpha} = 10\%$ NH_4CL hypoeutectic alloy, the solute NH_4CL is heavier than the solvent. The solutal expansion coefficient β_C is negative. The rejection of NH_4CL rich (water-lean) interdendritic fluid results in mutually augmenting solutal and thermal flows. A counter clockwise circulation is present in the mush and the liquid pool, Fig. 7a. The descending solute rich fluid tends to remain at the cavity bottom causing a weak reversal in the liquidus front development at the bottom of the cavity as can be seen in Fig. 7b, c. This is attributed as due to reduction of the local liquidus temperature.

At later times, time = 1200 s, when the melt width becomes narrow, circulation cells are observed to form along the liquidus interface as can be seen in Fig. 7b. These interfacial circulation cells move inward and upward (see Figs. 7b and 7c at time = 1200, 2000 s) with the passage of time. The advection of warmer fluid from the bulk melt to the mush, through the cells, combined with local NH_4CL enrichment by descending interdendritic fluid, favors remelting and development of flow channels. These channels form preferred paths for the solute rich fluid rejected from the mush.

The development of macrosegregation patterns at different times is shown in Fig. 8. Upon complete solidification (time = 8500 s), the channels manifest themselves in the form of V-segregates, which are areas of solute enriched bands adjacent to the solute depleted bands extending from the bottom to the top of the ingot. An area of positive segregation in the shape of an inverted cone is observed at the bottom of the cavity. Solute depleted zones along the ingot left wall with minimum NH_4CL concentration at the cavity top are also observed.

Rectangular ingot with a free surface

For $f_l^{\alpha} = 10\%$ NH_4CL, negative β_C, the rejection of NH_4CL rich (water-lean) interdendritic fluid results in mutually augmenting solutal and thermal flows inside the mushy region. Also, thermocapillary and diffuso-capillary effects induced due to temperature and concentration gradients on the free surface are augmenting each other.

Convection conditions after 870, 1200, and 2000 s of cooling are shown in Fig. 9. Contrasting Figs. 7 and 9, it is shown that the augmenting solutal, thermal, and capillary induced flows result in enhancing the flow intensity in the presence of a free surface. This can be inferred by comparing the maximum streamline values for each case. Also, the location of maximum flow intensity, represented by closely spaced streamlines, is shifted upward towards the cavity top as can be seen in Fig. 9a, b. In the presence of a free surface, maximum flow velocities are present near the cavity top, along the free surface and the liquidus interface. In the absence of a free surface, they are located near the liquidus interface. Flow circulation cells also develop in the presence of a free surface. However, the structure of flow pattern differs than the base case. This may be

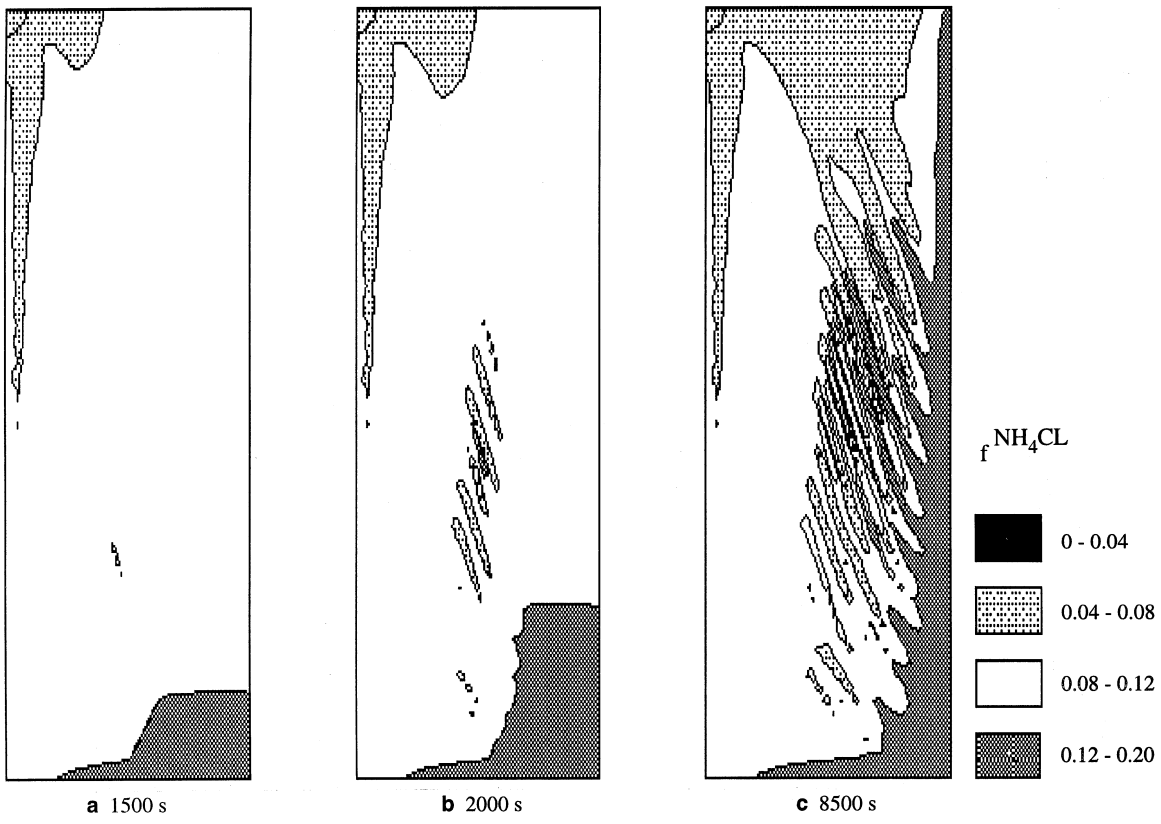

Fig. 8a–c. Development of macrosegregation with time during solidification of NH_4CL 10%-H_2O without a free surface

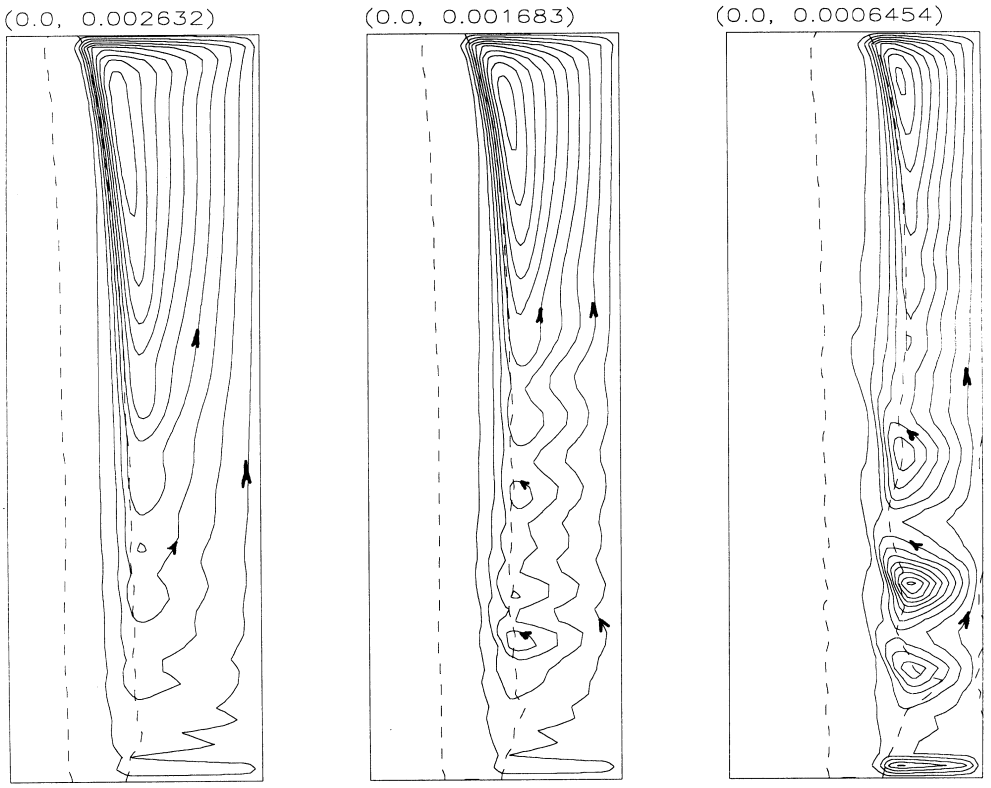

Fig. 9a–c. Convection conditions during solidification of NH_4CL 10%-H_2O with a free surface

attributed as due the increase of flow intensity and stretching of the main flow circulation towards the cavity top.

The development of macrosegregation patterns at different times is shown in Fig. 10. The V shaped segregates starts developing earlier in the presence of a free surface, as compared to the base case. This can be inferred by comparing Figs. 7a, b and 9a, b. Higher flow intensities in the presence of a free surface results also in higher degree of final macrosegregation. The variation of maximum and minimum H_2O concentration with time during solidification with and without a free surface is shown in Table 3. It is observed that, the value of minimum NH_4CL concentration decreases from 0.0535 and 0.0328 at 1200 s to 0.0 at complete solidification with and without a free surface, respectively. This is associated with the development of circulation cells at the liquidus interface and consequent V-segregates. The minimum values of NH_4CL concentration attained during solidification are smaller in the presence of a free surface. Maximum values of NH_4CL concentration are comparable for each case.

5 Conclusions

The important findings of the present study are summarized as follows.

Solidification of NH_4CL 70%-H_2O

Solidification of NH_4CL 70%-H_2O hypereutectic alloy in a side-chilled ingot without a free surface is characterized by a mushy zone for which the rejection of less dense water-rich interdendritic fluid results in solutally and thermally driven flows opposing each other. With the passage of time, the intensity of thermally induced flow decreases and solutally driven flow becomes dominant. Channels and "A segregates" develop early in the solidification process. Macrosegregation in the interior of the ingot is associated with large-scale fluid circulation through the mushy zone, which is driven by solutal buoyancy.

Table 3. Variation of minimum and maximum values of NH_4CL concentration with time during solidification of NH_4CL 10%-H_2O

Time (s)	240	390	870	1200	1500	2000	4000	8500
(a) Without a free surface								
$f_{min}^{NH_4CL}$	0.053	0.0535	0.0535	0.0535	0.0403	0.0035	0.0	0.0
$f_{max}^{NH_4CL}$	0.106	0.1192	0.1547	0.1755	0.1865	0.1901	0.1905	0.1969
(b) With a free surface								
$f_{min}^{NH_4CL}$	0.0561	0.0358	0.0338	0.0328	0.0098	0.00	0.00	0.00
$f_{max}^{NH_4CL}$	0.1062	0.1191	0.1548	0.17615	0.1861	0.1902	0.1917	0.1969

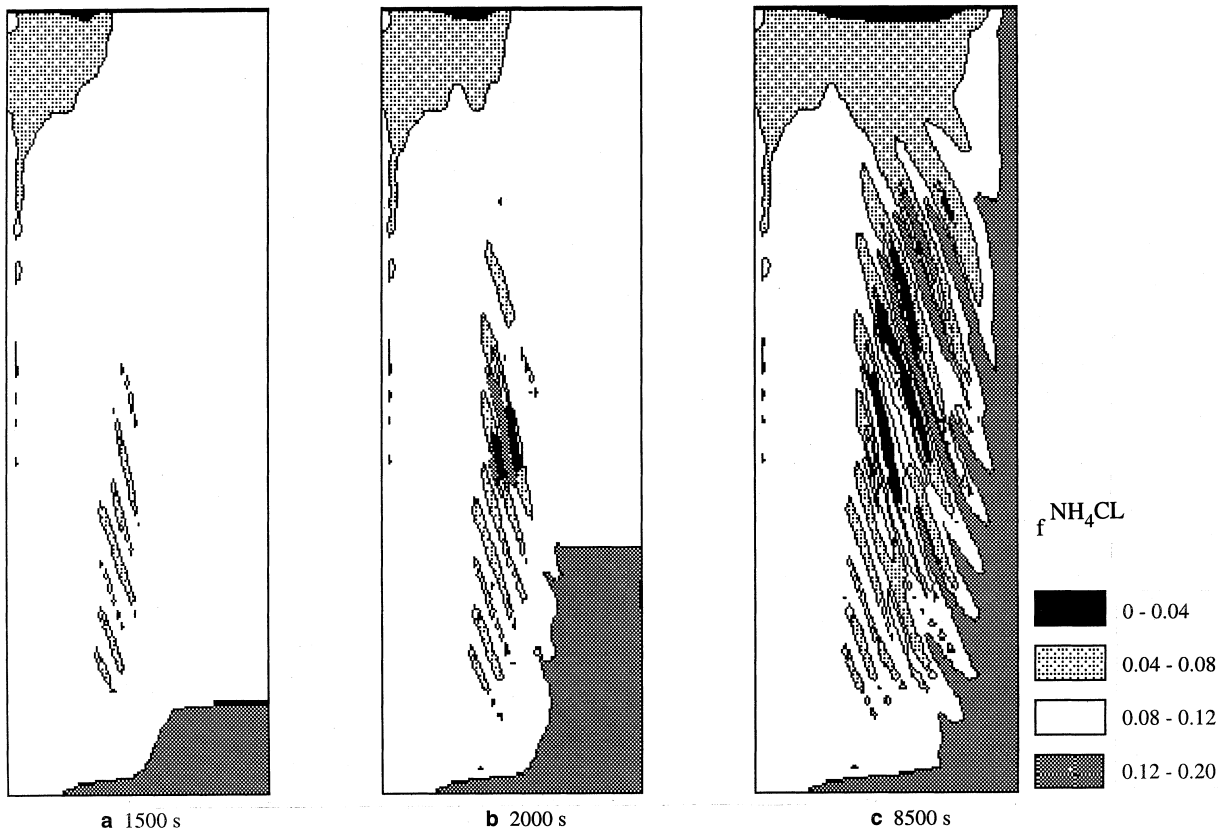

Fig. 10a–c. Development of macrosegregation with time during solidification of NH_4CL 10%-H_2O with a free surface

During solidification of NH_4CL 70%-H_2O hypereutectic alloy in a side-chilled ingot with a free surface, temperature and concentration gradients on the free surface create opposing thermocapillary and diffusocapillary effects. The dominant thermocapillary effects results in establishing a counterclockwise rotating cell at the cavity top, changing the number and orientation of developed channels, and creating an area of negative segregation at the cavity top.

Solidification of NH_4CL 10%-H_2O

During solidification of NH_4CL 10%-H_2O hypoeutectic alloy in a side-chilled ingot without a free surface, the rejection of NH_4CL rich (water-lean) interdendritic fluid results in mutually augmenting solutal and thermal flows. Large-scale flow circulation results in the formation of solute depleted zones at the cavity top and along the ingot left wall. A large area of positive segregation in the form of an inverted cone is observed in the interior of the ingot. Circulation cells at the liquidus interface that emerge at later stages of the process in the narrow melt are shown to be responsible for the development V-segregates.

During solidification of NH_4CL 10%-H_2O in a side-chilled ingot with a free surface, temperature and concentration gradients on the free surface induce augmenting thermocapillary and diffusocapillary effects. The intensity of flow is increased. The V shaped segregates start developing earlier in the presence of a free surface, as compared to the base case. Higher flow intensities in the presence of a free surface results also in a higher degree of final macrosegregation.

References

1. **McDonald RJ; Hunt JD** (1969) Fluid motion through the partially solid regions of a casting and its importance in understanding A Type segregation. TMS of AIME. 245: 1993–1997
2. **Bennon WD; Incropera FP** (1987) The evolution of macrosegregation in statistically cast binary ingots. Met. Trans. Vol. 18B, pp. 611–616
3. **Xu D; Li Q; Pehlke RD** (1991) Computer simulation of Al-Cu alloy solidification using a continuum model. AFS Trans. pp. 737–745
4. **Amberg G** (1991) Computation of macrosegregation in an Iron-Carbon cast. Int. J. of Heat Mass Transfer Vol. 34, pp. 217–227
5. **Viskanta R** (1988) Heat transfer during melting and solidification of metals. ASME J. Heat Transfer Vol. 110, pp. 1205–1219
6. **Rappaz M** (1989) Modeling of microstructure formation in solidification processes. Proc. of the Advanced Study Institute on Energy Optimization in Manufacturing and Materials Processing. IIT Madras, India, pp. 161–184
7. **Huppert HE** (1990) The fluid mechanics of solidification. J. Fluid Mech. Vol. 212, pp. 209–240
8. **Incropera FP; Viskanta R** (1992) Heat and mass transfer in materials processing. Hemisphere Pub. Corp. pp. 295–312
9. **Zebib A; Homsy GM; Meiburg E** (1985) High Marangoni Number convection in a square cavity. Phys. Fluids vol. 28, pp. 3467–3476
10. **Zehr RL; Chen MM; Muzumder J** (1987) Thermocapillary convection of a differentially heated cavity at high Marangoni Numbers. ASME paper 87-HT-29, presented at the National Heat Transfer Conference, Pittsburg, Pa.
11. **Kamotani Y; Ostrach S** (1987) Design of a thermocapillary flow experiment in reduced gravity. AIAA J. Thermophys. vol. 1, pp. 83–89

12. **Bergman TL** (1986) Numerical solution of double-diffusive Marangoni convection. Phys. Fluids vol. 29. pp. 2103–2108
13. **Bergman TL; Ramadhyani S** (1986) Combined buoyancy and thermocapillary driven convection in open square cavities. Numerical Heat Transfer vol. 9, pp. 441–451
14. **Munkata T; Tanasawa I** (1986) Buoyancy and surface tension driven natural convection with solidification. Proc. 8th Int. Heat Transfer Conf., eds. C.L. Tien, V.P. Carey, and H.K. farrell, vol. 4, pp. 1733–1738
15. **Keller JR; Bergman TL** (1988) Prediction of steady-state convection in solid/liquid system: Inclusion of buoyancy and surface tension effects in the liquid phase. ASME Proc. 1988, National Heat Transfer Conference, ed. H.R. Jacobs, vol.3, pp. 101–108
16. **Incropera FP; Engel AHH; Bennon WD** (1989) Numerical analysis of binary solid-liquid phase change with buoyancy and surface tension driven convection. Numerical Heat Transfer Part A, vol. 16, pp. 407–427
17. **Rady MA; Satyamurty VV; Mohanty AK** (1997) Thermos-olutal convection and macrosegregation during solidification of hypereutectic and hypoeutectic binary alloys in slatically cast trapezoidal ingots. Metallurgical and Materials Trans-action vol. 28B, pp. 943–952
18. **Bennon WD; Incropera FP** (1987) A continuum model for momentum, Heat and species Transport in Binary solid-liquid phase change systems- 1. Model formulation. Int. J. Heat Mass Transfer vol. 30, pp 2161–2170
19. **Prescott PJ; Incropera FP; Bennon WD** (1991) Modeling of dendritic solidification systems: Reassessment of the con-tinuum momentum equation. Int. J. Heat Mass Transfer vol. 34, pp. 2351–2359
20. **Bennon WD; Incropera FP** (1987) A continuum model for momentum, heat and species transport in binary solid-liquid phase change systems-II. Application to solidification in a rectangular cavity. Int. J. Heat Mass Transfer Vol. 30, pp. 2171–2187
21. **Rady MA** (1996) Studies on natural convection during melting and solidification of metals and alloys. Ph.D. Thesis, Mech. Eng. Dept., IIT Kharagpur, India
22. **Patankar SV** (1980) Numerical Heat Transfer and Fluid Flow, McGraw Hill, New York
23. **Rady MA; Mohanty AK** (1996) Natural convection during melting and solidification of pure metals in a cavity. Numerical Heat Transfer Part A, vol. 29, 49–63